Observation of Wave Packet Dichotomy and Adiabatic Stabilization in an Optical Waveguide

S. Longhi, M. Marangoni, D. Janner, R. Ramponi, and P. Laporta
Dipartimento di Fisica and Istituto di Fotonica e Nanotecnologie del CNR, Politecnico di Milano, Piazza L. da Vinci 32, I-20133 Milano, Italy

E. Cianci and V. Foglietti
Istituto di Fotonica e Nanotecnologie del CNR, sezione di Roma, Via Cineto Romano 42, 00156 Roma, Italy
(Received 11 November 2004; published 22 February 2005)

We report on the first experimental observation of wave packet dichotomy and adiabatic stabilization of light in a periodically bent optical waveguide in analogy with similar behavior of atoms in high-frequency strong laser fields.

DOI: 10.1103/PhysRevLett.94.073002 PACS numbers: 32.80.Rm, 42.50.−p, 42.82.Et

An atom subjected to an intense high-frequency laser field shows an exotic behavior which strongly deviates from the usual predictions of low-intensity laser-atom physics (see, e.g., Refs. [1,2], and references therein). One of the most spectacular of such deviations, first predicted by Pont, Gavrila, and co-workers in the study of atomic hydrogen driven by a high-frequency laser field [3], is the *adiabatic stabilization* of the atom, i.e., a surprising *increase* of the atom lifetime as the laser intensity *is increased* [4]. The adiabatic stabilization of the atom against ionization is associated with the appearance—for a linearly polarized field—of a dichotomous form for the electron cloud, i.e., a *splitting* of the ground state hydrogen wave function [3]. Many aspects of adiabatic stabilization and wave packet splitting can be understood by considering the electron dynamics in the Kramers-Henneberger (KH) reference frame—the rest frame of a classical electron in the laser field—where the atomic core appears to oscillate at the frequency of the driving laser field. Stabilization and wave packet splitting have their origin in the rapid motion of the atomic core potential so that, at leading order, the electron dynamics is governed by a cycle-averaged (dressed) potential [3], which supports a dichotomous stationary wave function. To date, the lack of adequate superintense and high-frequency lasers has not yet allowed the experimental observation of adiabatic stabilization and wave packet dichotomy of atomic hydrogen [5]; evidence in favor of stabilization has been reported considering low-lying Rydberg states [6] by measurements of anomalous ionization rates [7]. An experimental investigation of electron wave packet dynamics and the observation of wave packet dichotomy is of course not experimentally accessible in the atomic physics context. However, it has been recently suggested that similar behavior can be found in other physical systems which may allow for an easier experimental testing of the underlying dynamics, namely, in Bose-Einstein condensates subjected to a periodically shaken trap [8] and in an optical waveguide with a periodically bent axis [9]. In the latter case, light propagation along the waveguide is the optical analog of electron wave function evolution, the effect of the external laser field on the electron cloud being played by the periodic bending of the waveguide [9]. In this Letter, we present the first experimental observation of adiabatic stabilization and wave packet dichotomy of a light beam in a periodically bent optical waveguide which mimics similar dynamics of the electron cloud in a two-dimensional (2D) atom subjected to a high-frequency strong laser field. The sample realized for our experiments consists of a set of equal channel waveguides with a graded index profile fabricated by the annealed proton exchange (APE) technique in z-cut congruent lithium niobate [10]. The z axis of the waveguide is periodically bent along the x direction with a period $\Lambda = 160\ \mu$m and with a nonsinusoidal profile shown in Fig. 1(a). The amplitude $A(z)$ of the modulation is adiabatically increased from zero to a constant value $A_0 = 40\ \mu$m by a quarter sine-square envelope [Fig. 1(b)]. The total length of the waveguide is 3 cm and comprises a 0.5 cm-long section of straight waveguide,

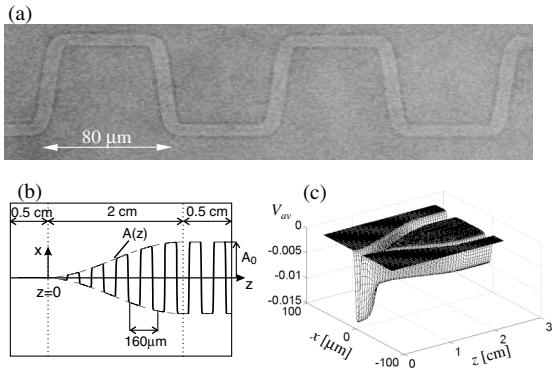

FIG. 1. (a) Microscope image (particular) of the periodically bent waveguide fabricated for the experiments. (b) Schematic of the full waveguide structure. (c) Numerically computed behavior of the average potential $V_{\rm av}(x, y, z)$ at $y = 0^+$ for parameter values which apply to our structure: $\Delta n = 0.0137$, $w = 5\ \mu$m, $D_x = 2.4\ \mu$m, $D_y = 3.5\ \mu$m, $n_s = 2.1381$.

which enables excitation of the straight waveguide mode, a 2 cm-long adiabatic section in which the amplitude of the bending is slowly increased up to 40 μm, and a final 0.5 cm-long section of bent waveguide with constant modulation amplitude [Fig. 1(b)]. The waveguide was probed at three different wavelengths ($\lambda = 633$, 1064, and 1550 nm) using single-mode lasers; the waveguide turns out to be single mode at $\lambda = 1550$ nm and multimode at the two other wavelengths. Light coupling was accomplished by focusing the circular diffraction-limited TEM_{00} Gaussian laser radiation into the input face of the waveguide through a 25× microscope objective to obtain a $\simeq 3.5$ μm focused spot size radius. The polarization of the incident beam was set orthogonal to the plane of the waveguide in order to couple the TM modes supported by the APE waveguide. The transverse light beam distribution at the exit of the sample was imaged onto an infrared Vidicon camera and analyzed using a beam profiler software. The waveguide refractive index profile is given by $n(x, y, z) = n(x - x_0(z), y)$, where $n(x, y)$ is the refractive index of the channel straight waveguide and $x_0(z)$ is the bending profile of the waveguide axis shown in Fig. 1(b). The explicit expression for $n^2(x, y)$ reads $n^2(x, y) = n_c^2 \simeq 1$ for $y < 0$ (in the air) and $n^2(x, y) = n_s^2 + 2n_s\Delta n g(x) f(y)$ for $y > 0$ (in the substrate), where n_s is the extraordinary refractive index of the substrate, $\Delta n \ll n_s$ is the peak index change, and $g(x)$ and $f(y)$ define, respectively, the shape of the index profile parallel to the surface of the waveguide (x direction) and perpendicular to the surface (y direction). For the fabrication process of our waveguide, the shape of $g(x)$ and $f(y)$ can be expressed as $g(x) = \{\mathrm{erf}[(x + w)/D_x] - \mathrm{erf}[(x - w)/D_x]\}/[2\,\mathrm{erf}(w/D_x)]$ and $g(y) = \exp(-y/D_y)$, where $2w$ is the channel width and D_x and D_y are the lateral and in-depth diffusion lengths [11]. Light propagation along the waveguide can be well described by the scalar Helmholtz equation $\partial^2 E/\partial z^2 + \nabla_\perp^2 E + k^2 n^2(x - x_0(z), y)E = 0$ for the electric field amplitude $E(x, y, z)$, where $k = 2\pi/\lambda$ is the wave number (in vacuum) of the injected light and $\nabla_\perp^2$ is the transverse Laplacian. After setting $E(x, y, z) = \psi(x, y, z)\exp(ikn_s z)$ and introducing the paraxial approximation ($|\partial^2\psi/\partial z^2| \ll kn_s|\partial\psi/\partial z|$), one obtains for the envelope ψ the following propagation equation:

$$i\lambda\frac{\partial\psi}{\partial z} = -\frac{\lambda^2}{2n_s}\nabla_\perp^2\psi + V(x - x_0(z), y)\psi, \qquad (1)$$

where we have set $\lambda \equiv \lambda/(2\pi)$ and $V(x, y) \equiv [n_s^2 - n^2(x, y)]/(2n_s) \simeq n_s - n(x, y)$. As noticed in [9], with the formal substitution $z \to t$, $\lambda \to \hbar$, and $n_s \to m$, Eq. (1) is the semiclassical Schrödinger equation, in the KH frame, for a 2D electron in the binding potential $V(x, y)$, subjected to an external field linearly polarized along the x axis. The oscillating term $x_0(z)$, which represents the quiver motion of a classical electron subjected to the external field [3], can be represented by the product of the rapidly varying periodic function $f(z)$, shown in Fig. 1(a), with the slowly varying envelope $A(z)$ shown in Fig. 1(b), i.e., $x_0(z) = A(z)f(z)$. In the atomic analogy, this envelope may account for a smooth turn on of the laser pulse [12]. Wave packet dichotomy is observable in the high-frequency modulation regime, where at leading order the electron dynamics may be described by a cycled-average potential, provided that the classical excursion of the electron be large enough compared to the size of the unperturbed atom [2,3]. The high-frequency limit leads to the averaged wave equation [9]:

$$i\lambda\frac{\partial\psi}{\partial z} = -\frac{\lambda^2}{2n_s}\nabla_\perp^2\psi + V_{\mathrm{av}}(x, y, z)\psi, \qquad (2)$$

where

$$V_{\mathrm{av}}(x, y, z) = \frac{1}{\Lambda}\int_0^\Lambda dz' V(x - A(z)f(z'), y) \qquad (3)$$

is the cycled-averaged potential. Note the dependence of V_{av} on z, which comes from the slow ramp envelope $A(z)$ in the adiabatic section of the waveguide. The behavior of $V_{\mathrm{av}}(x, y, z)$ at $y = 0^+$ for the fabricated waveguide is depicted in Fig. 1(c), which clearly corresponds to an adiabatic Y branch waveguide [13]. Wave packet splitting can be thus explained, in the optical analogy, as due to the existence of a Y branch in the averaged waveguide model. The effect of the adiabatic waveguide section is to slowly create the branch point where beam splitting occurs. Waveguide losses, corresponding in the atomic analogy to ionization, cannot be accounted for by the simple averaged waveguide model; however, they can be numerically computed by a direct integration of Eq. (1) on a finite transverse domain using absorbing boundary conditions [9]. The period Λ and modulation depth A_0 of waveguide bending were designed such that the conditions for adiabatic stabilization are approximately met when the waveguide is illuminated at $\lambda = 1.55$ μm, but not at $\lambda = 633$ nm, where the guiding properties of the structure are fully lost. The $\lambda = 1064$ nm wavelength corresponds to a transition case where beam splitting may still be observed, though with higher radiation losses and the possibility to excite higher-order modes [14]. In Fig. 2 we show experimental results obtained when the waveguide is excited at $\lambda = 1550$ nm, together with numerical simulations of Eq. (1) [15]. Figures 2(b) and 2(d) show the measured beam intensity pattern at the output facet of the waveguide [Fig. 2(b)] and corresponding profile [Fig. 2(d)] obtained by sectioning the two-spot pattern along the horizonal x direction. Note that the two well-resolved spots in the figures are separated by $\simeq 80$ μm, i.e., by the full modulation depth $2A_0$. By estimating laser mode coupling into the waveguide mode of the order of 85% and by taking into account additional 25% Fresnel losses at the input and output interfaces of the sample, the measured internal

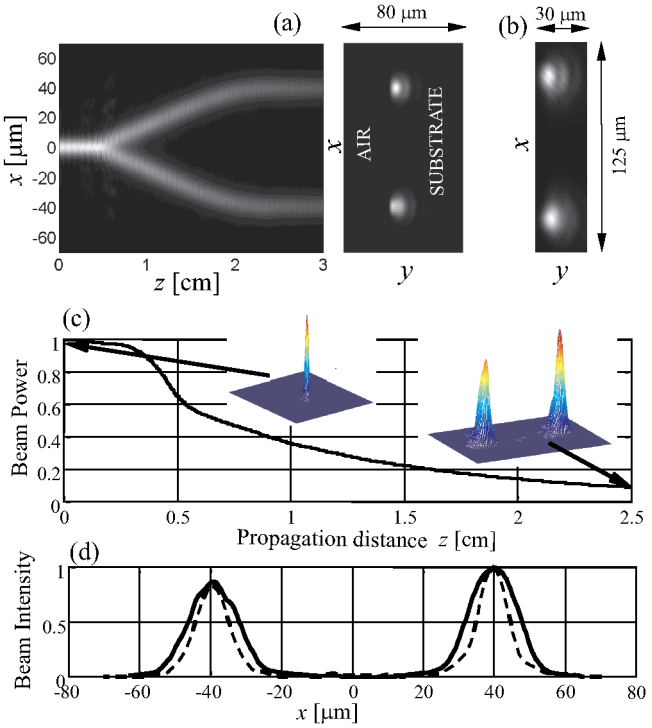

FIG. 2 (color online). (a) Light propagation along the waveguide (top view) and corresponding intensity pattern at the output plane as obtained by numerical simulation of Eq. (1) when the waveguide is probed at $\lambda = 1550$ nm in its fundamental mode. (b) Intensity pattern of light at the output plane of the waveguide as recorded on the infrared camera. (c) Numerically computed beam power $\mathcal{P}$ (in arbitrary units) versus propagation distance z showing radiation losses. The insets show the 2D intensity patterns at the input and output planes of the waveguide. (d) Experimentally measured intensity profile (in arbitrary units) of the output light beam taken along the horizontal x direction (solid curve) and corresponding profile as obtained by numerical simulations (dotted curve).

transmission of the waveguide at $\lambda = 1550$ nm was measured to be $\simeq 10\%$. The experimental results were reproduced for different waveguides in the sample, obtaining the same splitting behavior and comparable values for internal transmission. Figure 2(a) shows the evolution of the horizontal light field amplitude $|\psi(x, y = 0, z)|$ along the waveguide (top view of the waveguide) and corresponding transverse beam intensity pattern at the exit of the waveguide, as obtained by numerical simulations when the injected beam is the fundamental mode of the straight waveguide. Note that beam splitting occurs in the adiabatic section of the waveguide when the ramp term $A(z)$ becomes comparable with the width ($\sim 2w$) of the waveguide channel. Figure 2(c) shows the evolution, along the propagation distance z, of the normalized beam power $\mathcal{P} = \int dxdy|\psi(x, y, z)|^2$ internal to the integration domain. The insets of the figure depict the 2D beam intensity profile at the input and output planes of the waveguide. The internal transmission of the waveguide estimated from

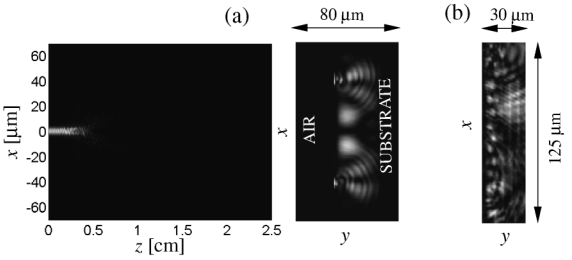

FIG. 3. Same as Figs. 2(a) and 2(b) but when the waveguide is probed at $\lambda = 633$ nm.

the numerical results is thus $\simeq 9.5\%$, in good agreement with the experimental measurement. Note that, as expected, radiation losses are higher at the beginning of the adiabatic waveguide section; however, even in the final uniform section of the waveguide, one can observe radiation losses, which cannot be accounted for by the averaged waveguide model (2). Analogously, the slight asymmetry of the two output spots, observed in the experiment and well reproduced by numerical simulations [see Fig. 2(d)], can be ascribed to a breakdown of the averaged waveguide approximation, i.e., to the fast periodic alternation of guiding/diffraction experienced by the two splitted spots during propagation [see Fig. 1(a)] in a similar way to what happens in a periodically segmented waveguide [16]. Figures 3–5 show the results obtained when the waveguide was probed with radiation at $\lambda = 633$ nm (Fig. 3) and $\lambda = 1064$ nm (Figs. 4 and 5). At these wavelengths, the straight waveguide is not single mode so that, depending on the focusing conditions of the injected beam, higher-order modes (or a superposition of modes) may be excited [14]. For the $\lambda = 633$ nm case a noisy pattern [Fig. 3(b)] was always observed, regardless of the focusing condi-

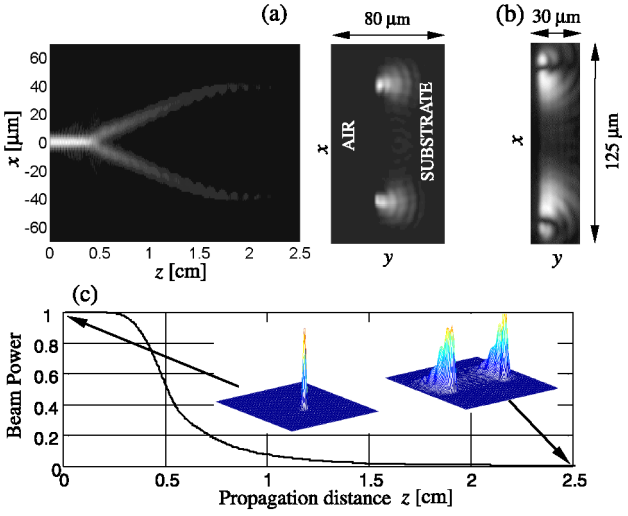

FIG. 4 (color online). Same as Figs. 2(a)–2(c) but when the waveguide is probed at $\lambda = 1064$ nm. Numerical simulations shown in (a) and (c) are obtained when the fundamental TM_{00} waveguide mode is excited.

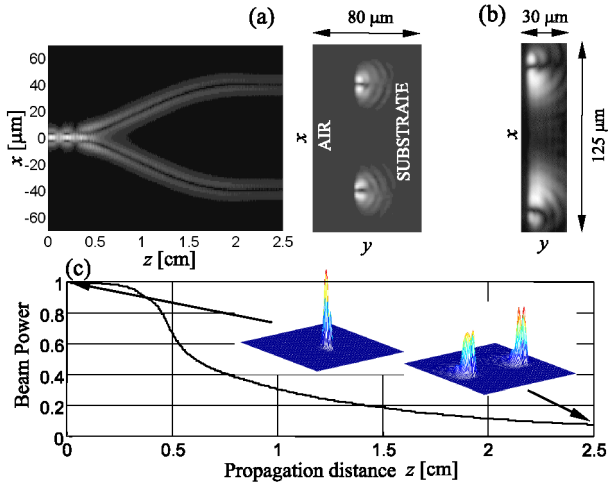

FIG. 5 (color online). Same as Fig. 4 but numerical simulations in (a) and (c) are now obtained when the first-order TM_{10} waveguide mode is excited. The experimental measurement in (b) is the same as in Fig. 4(b) and reported for the sake of comparison with numerical results.

tions, indicating high losses for the waveguide. This is in agreement with the numerical simulations [Fig. 3(a)], which indicate that the bending of waveguide produces strong losses in the first section of the adiabatic region (at around $z = 3.5$ mm), with an internal transmission of the waveguide less than 0.5×10^{-3}. At $\lambda = 1064$ nm wavelength excitation, beam splitting was experimentally observed [see Fig. 4(b)], with a measured internal transmission of the waveguide reduced to $\simeq$1.8%, i.e., about one fifth as compared to excitation at $\lambda = 1550$ nm. Note that the shape of each spot at the output facet of the waveguide shows a nearly two-lobe structure, which is a signature of a multimode regime as opposed to the $\lambda = 1550$ nm excitation case [compare Figs. 4(b) and 2(b)]. Since the first straight waveguide section is multimode at $\lambda = 1064$ nm, when light is coupled into the waveguide a superposition of low-order modes is presumably excited, with a higher weight for the fundamental waveguide mode at optimum alignment conditions; the splitted beams at the output may be hence considered as a mixture of propagated waveguide modes initially excited in the structure. The numerical simulations shown in Figs. 4(a), 4(c), 5(a), and 5(c) show, as an example, the propagation properties of the waveguide excited by the fundamental TM_{00} and first-order (in the vertical y direction) TM_{10} waveguide modes. Note that, rather surprisingly, the radiation losses of the bent waveguide are sensitively *lower* for the TM_{10} mode rather than for the fundamental TM_{00} mode (internal transmission is $\simeq$7.5% and $\simeq$0.8% in the two cases, respectively). Note also that the excitation of the TM_{10} mode leads, after propagation [see the insets of Fig. 5(c)], to the appearance of a two-lobe structure for each spot in the *horizontal* x direction, as observed in the experimental measurement [compare Figs. 5(a) and 5(b)]. In conclusion, our results provide for the first time clear evidence, in an experimentally accessible optical system, of the exotic phenomenon of electron wave function dichotomy encountered in strong laser-atom physics.

[1] M. Gavrila, in *Atoms in Intense Laser Fields*, edited by M. Gavrila (Academic Press, New York, 1992), p. 435; K. Burnett, V. C. Reed, and P. L. Knight, J. Phys. B **26**, 561 (1993); M. Protopapas, C. H. Keitel, and P. L. Knight, Rep. Prog. Phys. **60**, 389 (1997).
[2] M. Gavrila, J. Phys. B **35**, R147 (2002).
[3] M. Pont, N. R. Walet, M. Gavrila, and C. W. McCurdy, Phys. Rev. Lett. **61**, 939 (1988).
[4] M. Pont and M. Gavrila, Phys. Rev. Lett. **65**, 2362 (1990).
[5] M. Dondera, H. G. Muller, and M Gavrila, Phys. Rev. A **65**, 031405(R) (2002).
[6] R. J. Vos and M. Gavrila, Phys. Rev. Lett. **68**, 170 (1992).
[7] M. P. de Boer, J. H. Hoogenraad, R. B. Vrijen, L. D. Noordam, and H. G. Muller, Phys. Rev. Lett. **71**, 3263 (1993); N. J. van Druten, R. C. Constantinescu, J. M. Schins, H. Nieuwenhuize, and H. G. Muller, Phys. Rev. A **55**, 622 (1997).
[8] R. Dum, A. Sanpera, K.-A. Suominen, M. Brewczyk, M. Kus, K. Rzazewski, and M. Lewenstein, Phys. Rev. Lett. **80**, 3899 (1998).
[9] S. Longhi, D. Janner, M. Marano, and P. Laporta, Phys. Rev. E **67**, 036601 (2003).
[10] M. L. Bortz and M. M. Fejer, Opt. Lett. **16**, 1844 (1991).
[11] A. Sharma and P. Bindal, Opt. Quantum Electron. **24**, 1359 (1992).
[12] Q. Su, J. H. Eberly, and J. Javanainen, Phys. Rev. Lett. **64**, 862 (1990).
[13] The choice of a nonsinusoidal waveguide bending profile, which in the atomic analogy corresponds to a driving laser field containing higher-order harmonics, is motivated by the need to get a well pronounced two-peaked structure for $V_{\rm av}$, allowing for a clear observation of wave packet dichotomy at the waveguide output plane.
[14] Excitation of higher-order waveguide modes corresponds, in the atomic analogy, to consider excited bound states for the electron wave function.
[15] Equation (1) was integrated by a standard beam propagation pseudospectral technique on a rectangular 140 μm $\times$ 80 μm domain with absorbing boundary conditions and using 256×256 spectral modes.
[16] Z. Weissman and A. Hardy, J. Lightwave Technol. **11**, 1831 (1993).